



# Far-Field Tsunami Hazard Assessment Along the Pacific Coast of Mexico by Historical Records and Numerical Simulation. Part II: Tsunami-Induced Currents in the Port of Ensenada, Baja California

LAURA G. ORTIZ-HUERTA<sup>1</sup> 

**Abstract**—The time evolution of the velocity field in and around the Port of Ensenada, induced by large distant tsunamis as produced by Mw 9.3 hypothetical earthquakes around the Pacific Ocean, is analyzed through the numerical modeling of distant tsunamis. The results indicate that tsunami-induced currents are 4–6 knots ( $\sim 2$  to 3 m/s) at the harbor entrance and 2–4 knots ( $\sim 1$  to 2 m/s) inside and outside the harbor. Low amplitude tsunamis, as well as the reverberance or coda of large distant tsunamis, may produce currents of 2 knots ( $\sim 1$  m/s) along the harbor channel induced by the interaction of coastal and harbor seiches. Visual scrutiny of the resulting velocity field at time steps of 1 min, as well as the mathematical concept of residual velocity, reveal transient eddies fed by flood and ebb currents that produce transversal currents by the harbor entrance. Currents induced by large distant tsunamis are practically negligible at depths greater than 120 m (15 km offshore from the harbor).

**Key words:** Port of Ensenada, distant tsunamis, velocity field, harbor seiches, numerical modeling.

## 1. Introduction

The Port of Ensenada, Baja California, Mexico, located in the northwestern part of the Peninsula of Baja California (116.62°W; 31.85°N; Fig. 1), is considered to be one of the most important ports along the Pacific Coast of Mexico. This port is attending large cargo and touristic vessels ( $\sim 300$  m long;  $\sim 70,000$  Tons), as well as fishing ships and small vessels (e.g., [www.puertoensenada.com.mx](http://www.puertoensenada.com.mx)). Despite being located in a seismically active region, no local or regional generated tsunamis have been noticed in the short time history of Ensenada ( $\sim 137$  years). In contrast,

historical as well as recent distant tsunamis produced by large earthquakes around the Pacific Ocean have been well documented in the Port of Ensenada (Fig. 2; Table 1). Among them, the historic Chile (22 May 1960,  $M_w$  9.5), and Alaska (27 March 1964,  $M_w$  9.3) tsunamis produced the most significant water levels observed in the port. Since the Intergovernmental Coordination Group for the Pacific Tsunami Warning System (ICG/PTWS) started operations in 1965 (ITSU Master Plan 1999), no formal tsunami warnings were issued at that time. Nonetheless, for the Alaska 1964 tsunami, a particular telephone call was received from the Port of San Diego, California, telling that Kodiak, Alaska, was devastated by a strong earthquake, and that a seismic tidal wave was in progress in the Pacific. At that time, harbor operations in the Port of Ensenada consisted mainly in attending the tuna fishing fleet and the floating dock for their maintenance. As such, the primary objective during the arrival of the Alaska tsunami was to secure the floating dock by tightening and releasing its moorings from pier #1 according to the demand imposed by the tsunami-induced water level variations. Most of the inhabitants in the port neighborhood evacuated to the hills where they spent the night until the next morning after seeing for themselves that nothing happened in the harbor (Port Captain J. Prieto-Guzman, inedited narrative, 1964).

As for the recent Tohoku tsunami (11 March 2011,  $M_w$  9.0), port authorities in Ensenada indicated that, since the tsunami would arrive during the neap tide period, it would be contained between high and low tide levels, thereby reducing the inundation impact. However, large cargo and tourism vessels evacuated to open sea as a precautionary measure after seen the striking images of the Tohoku tsunami

<sup>1</sup> Instituto de Investigaciones Oceanológicas, Universidad Autónoma de Baja California (UABC), Ensenada, Baja California, Mexico. E-mail: [laura\\_ortiz@uabc.edu.mx](mailto:laura_ortiz@uabc.edu.mx); [lortiz.huerta@gmail.com](mailto:lortiz.huerta@gmail.com)

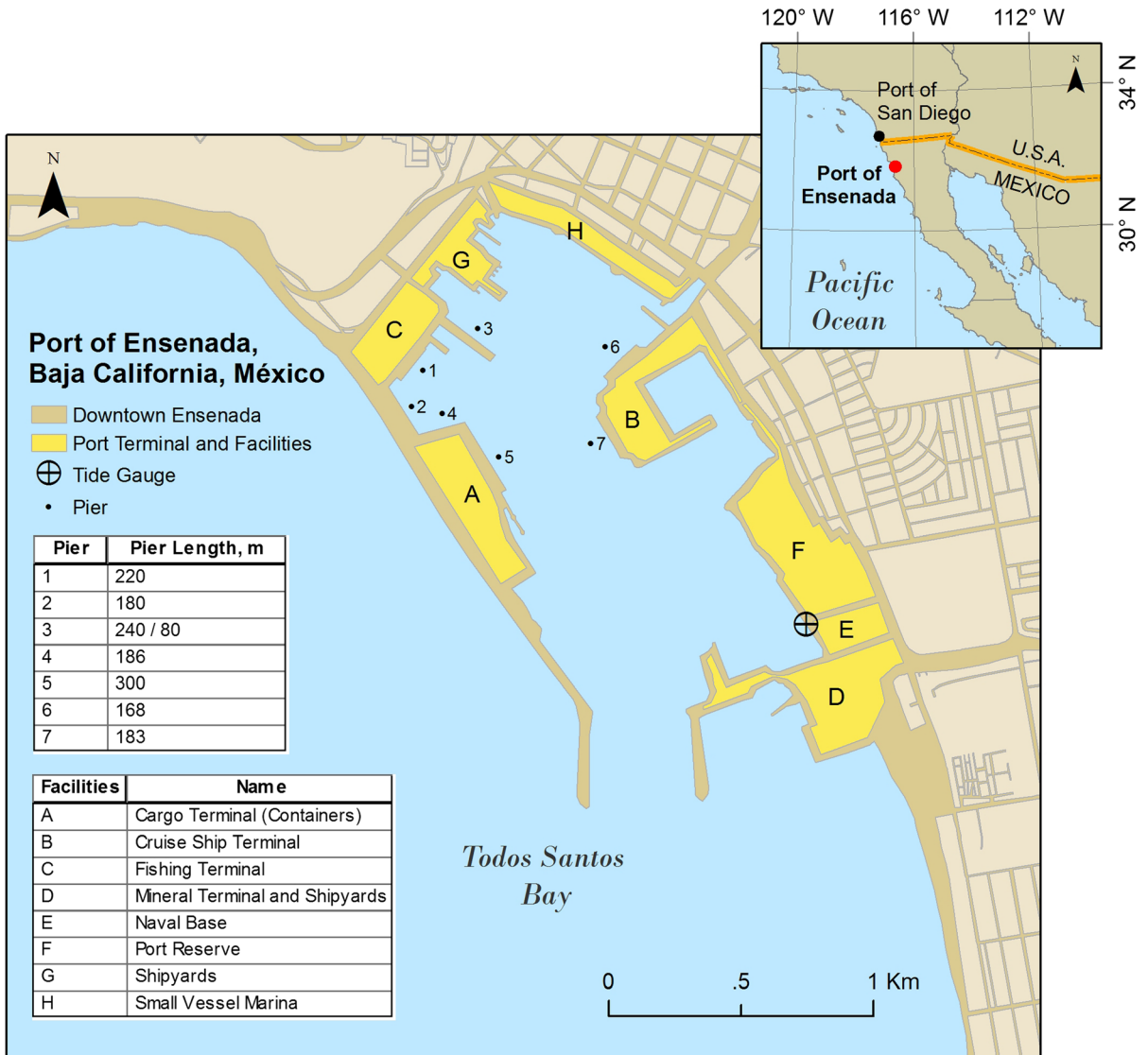


Figure 1  
Map and facilities of the Port of Ensenada, Baja California, Mexico

broadcasted live by the NHK World-Japan television network. Because the tsunami arrived during the daylight hours, strong currents and eddies were observed for the first time by myself and other eyewitnesses for several hours, as traced by floating debris and suspended sediments at the port entrance. During the Chile tsunami (27 February 2010,  $M_w$  8.8) the port was closed to navigation but reopened a few hours after the arrival of the tsunami, given that the effects within the port were considered practically unharmed. During the remaining tsunamis illustrated

in Fig. 2, the Port of Ensenada remained open to navigation after the tsunami advisories were issued by the Pacific Tsunami Warning Center.

In addition to the tsunami inundation hazard, harbors are naturally vulnerable to tsunami-induced currents and, consequently, to the potential damage by drifting structures of varying sizes. As for the tsunami experiences in the Port of Ensenada, harbor operations have been guided solely by empirical knowledge. Therefore, an analysis of expected tsunami-induced currents is necessary to anticipate harbor operations as well as

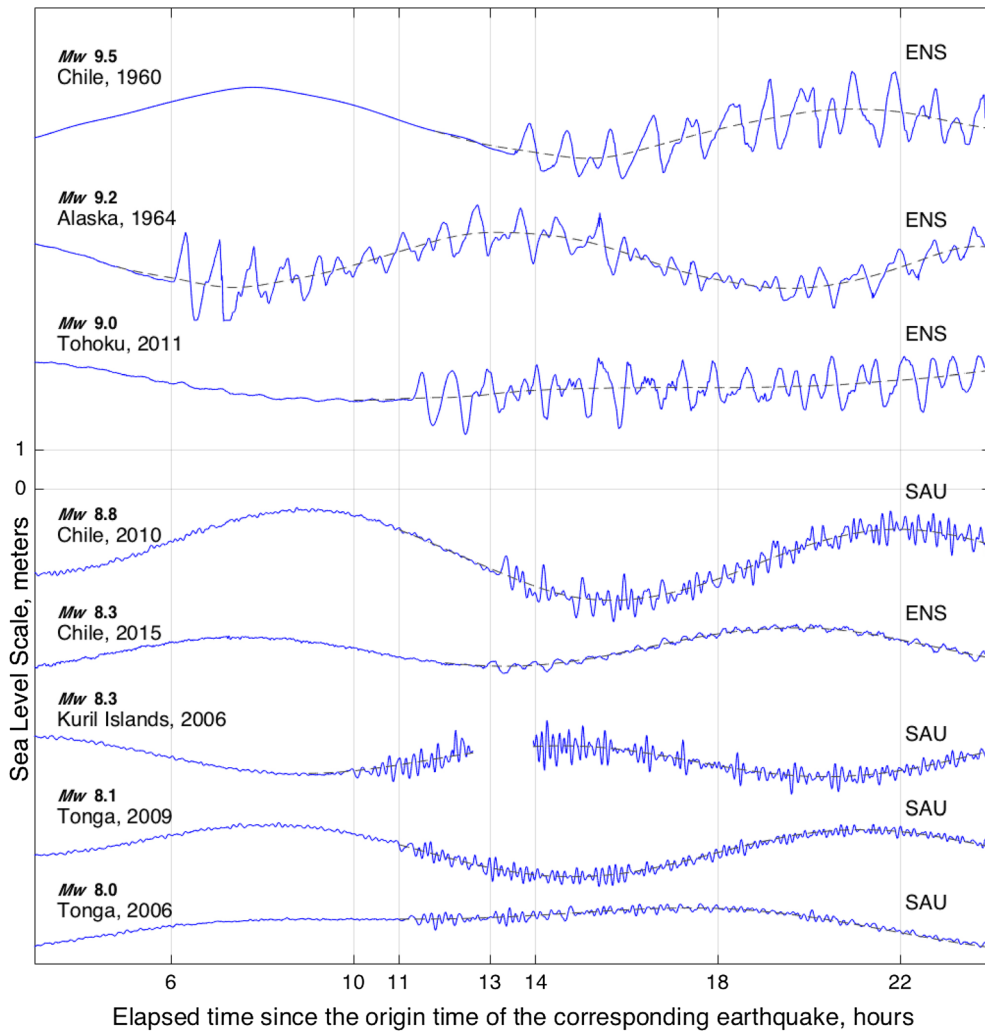


Figure 2

Historical and recent tsunami records recorded in Todos Santos Bay at the Ports of Ensenada (ENS), and Sauzal (SAU), Baja California, Mexico. Dashed lines indicate the corresponding predicted tide. The origin region and the magnitude of the earthquakes are indicated in the corresponding marigram or sea level record. See Fig. 5 for locations of Ensenada and Sauzal in Todos Santos Bay

Table 1

Basic statistics of the tsunami records illustrated in Fig. 2

	Chile 1960	Alaska 1964	Tohoku 2011	Chile 2010	Chile 2015	Kuril 2006	Tonga 2009	Tonga 2006
$H_s$ (m)	1.57	1.28	1.26	0.79	0.22	0.69	0.39	0.28
$T_s$ (min)	57	45	43	14	24	8	10	13
Max $H$ (m)	1.91	2.21	1.82	0.97	0.31	1.00	0.60	0.44

$H_s$  is the significant wave height (crest to trough) or the average height of the highest one-third waves during the first 12 h after the tsunami arrival and  $T_s$  is the significant wave period or the average zero-crossing wave period of the highest one-third waves

safety maritime evacuation zones as a guideline to the establishment of a tsunami response harbor operation plan.

Here after, tsunami-induced currents will be expressed in knots which are more familiar to navigators to whom this study is addressed.

## 2. Numerical Modeling of Distant Tsunamis

A comprehensive analysis of expected tsunami hazard along the Pacific Coast of Mexico for distant tsunamis, originated by  $M_w \sim 9.3$  synthetic earthquakes around the Pacific Ocean, indicates that tsunami heights in the Port of Ensenada are expected to be 1–2.5 m above the still water level (Ortiz-Huerta et al. 2018). Therefore, two case scenarios of tsunami-induced currents in the Port of Ensenada are presented in this study as thresholds representatives of the 23 tsunami-case scenarios analyzed in Ortiz-Huerta et al. (2018). The upper threshold scenario corresponds to a tsunami originated by an earthquake in the Aleutian Trench aside of the western edge of the 27 March 1964 Alaska earthquake, while the lower threshold scenario corresponds a tsunami originated above the rupture area of the 11 March 2011 Tohoku earthquake (regions 3 and 11 respectively, in Ortiz-Huerta et al. 2018). The focal mechanism of the earthquakes in both case scenarios is prescribed here by the FOCAL-II dislocation model defined by a uniform slip distribution of 20 m on a rectangular large thrust fault ( $600 \times 180 \text{ km}^2$ ) dipping  $15^\circ$  at the depth of 20 km. The goodness of the FOCAL-II dislocation model was probed to be adequate for the numerical simulation of large distant tsunamis, such as the ones produced by the Chile 1960, Alaska 1964, and Tohoku 2011 earthquakes (Ortiz-Huerta et al. 2018).

The transoceanic propagation modeling of the tsunami in both case scenarios is computed with the numerical tsunami propagation model of Goto et al. (1997), which solves the vertically integrated (depth-averaged) linearized shallow water momentum and continuity equations or linear long wave equations in a rotating Earth (e.g., Dronkers 1964; Pedlosky 1979):

$$\frac{\partial \eta}{\partial t} + \nabla \cdot \mathbf{M} = 0, \quad (1)$$

$$\frac{\partial \mathbf{M}}{\partial t} + 2\boldsymbol{\Omega} \times \mathbf{M} + gh\nabla\eta = 0. \quad (2)$$

In Eqs. (1, 2),  $t$  is time,  $\eta$  is the vertical displacement of the water surface above the still water level (the equipotential surface),  $h$  is the ocean depth,  $g$  is the gravitational acceleration and  $\boldsymbol{\Omega}$  is the angular

velocity of the Earth.  $\mathbf{M} = [U, V]$  is the horizontal depth-averaged volume flux vector, where  $U = u(\eta + h)$  and  $V = v(\eta + h)$  are the horizontal depth-averaged volume flux vectors in longitudinal and latitudinal spherical coordinates, and  $u$  and  $v$  are the corresponding water particle velocities.

The above set of Eqs. (1, 2) are solved by finite differences in an explicit staggered leap-frog scheme at time steps of 2 s in a spatial grid resolution of 2 min. The current bathymetry or domain of integration of the numerical model for the transoceanic tsunami propagation corresponds to the ETOPO2v2 dataset (National Geophysical Data Center 2006) in a matrix of  $5761 \times 3891$  nodes.

In both case scenarios, the tsunami initial condition or sea surface deformation was taken as the vertical deformation of the seafloor produced by the FOCAL-II dislocation model, as computed by the expression given by Mansinha and Smylie (1971).

The modeling of the tsunamis in the target region is computed at time steps of 2 s in a set of interconnected nested grids within the transoceanic domain of integration (grid resolution 38 m, Fig. 3; grid resolution 353 m, Fig. 5), where full non-linear terms (advective and bottom friction) are included in the expressions (3, 4) of Eqs. (1, 2) in a rectangular coordinate system  $(x, y)$ , disregarding Coriolis terms:

$$\frac{\partial \eta}{\partial t} + \frac{\partial U}{\partial x} + \frac{\partial V}{\partial y} = 0 \quad (3)$$

$$\begin{aligned} \frac{\partial U}{\partial t} + \frac{\partial}{\partial x} \left( \frac{U^2}{D} \right) + \frac{\partial}{\partial y} \left( \frac{UV}{D} \right) + gD \frac{\partial \eta}{\partial x} \\ + \frac{gn^2}{D7\beta} U \sqrt{U^2 + V^2} = 0, \\ \frac{\partial V}{\partial t} + \frac{\partial}{\partial x} \left( \frac{UV}{D} \right) + \frac{\partial}{\partial y} \left( \frac{V^2}{D} \right) \\ + gD \frac{\partial \eta}{\partial y} + \frac{gn^2}{D7\beta} V \sqrt{U^2 + V^2} = 0. \end{aligned} \quad (4)$$

The Gauckler–Manning roughness coefficient  $n$  in the bottom friction terms (Eqs. 4) was set to 0.025 (cf., Titov et al. 2003).

The Shallow Water Model Equations (Eqs. 3, 4) has been widely used to adequately reproduce tsunami records recorded in tide gauges in bays and

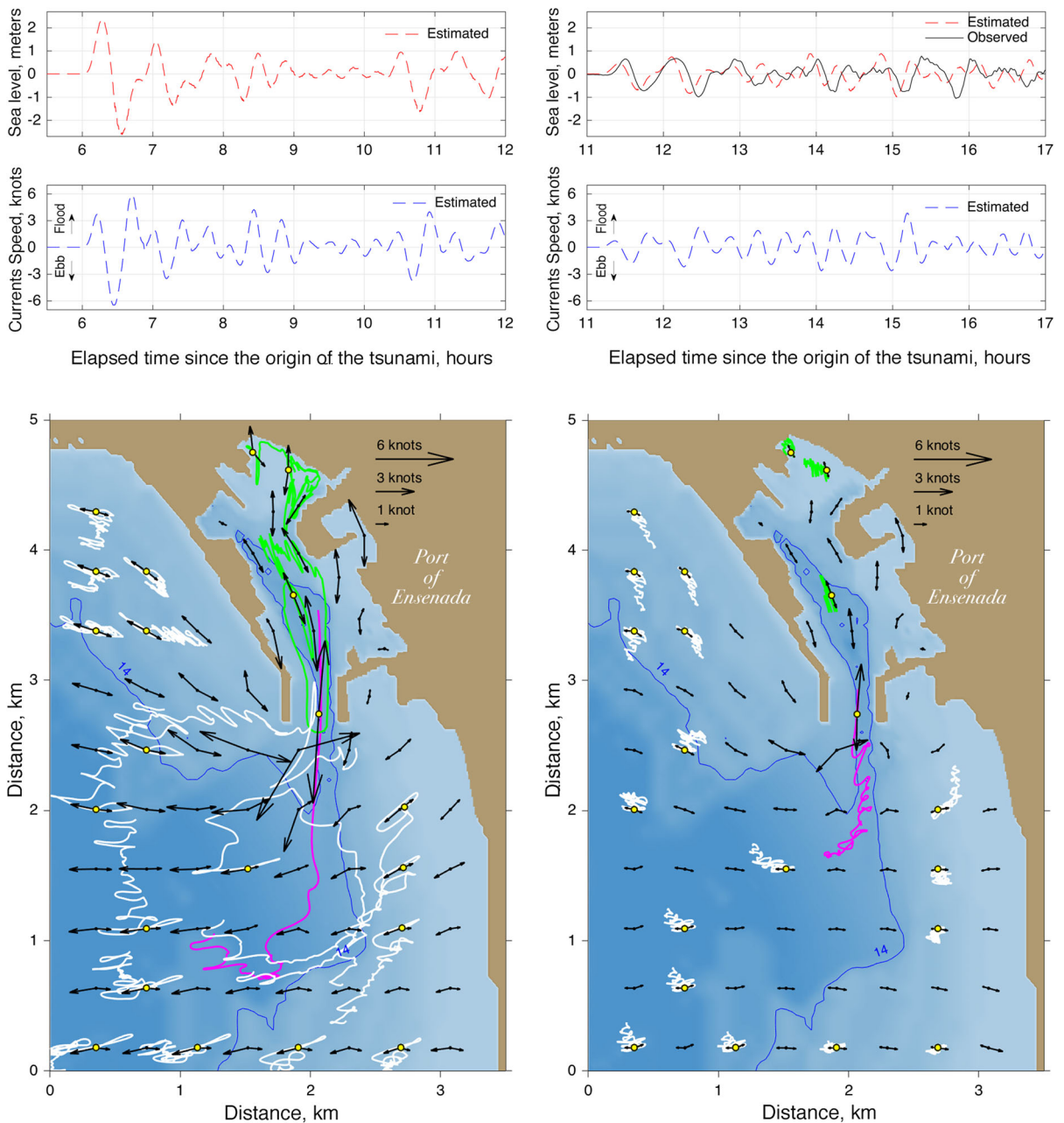


Figure 3

Left panels (upper threshold scenario); Right panels (lower threshold scenario). Upper panels: sea level and currents at the harbor entrance. Lower panels: maximum flood and ebb currents inside and around the harbor reached during the first 6 h after the tsunami arrival. Yellow dots at the base of velocity vectors indicate the initial position of water particle Lagrangian paths. White lines indicate Lagrangian paths outside the harbor; green inside the harbor and the magenta line indicate the path departing from the harbor entrance. The 14 m isobath is depicted in blue

harbors. Recently, a large of number of records of tsunami-induced currents by the Tohoku 2011 tsunami, recorded in bays and harbors, have allowed the

validation of the deep-averaged equations to adequately reproduce the time evolution of velocity fields (e.g., Arcos and LeVeque 2015).

### 3. Tsunami-Induced Currents in the Port of Ensenada

The time evolution of the velocity field in and around the harbor resulting from the numerical model is examined here at time steps of 1 min. The resulting tsunami-induced currents in both case scenarios is illustrated in Fig. 3. Currents in the upper threshold scenario reached 6 knots at the harbor entrance and 2–4 knots inside and outside the harbor, while currents in the lower threshold scenario reached 4 knots at the harbor entrance and 1–3 knots inside and outside the harbor. Note that the observed marigram of the 11 March 2011 Tohoku tsunami is also traced in Fig. 3 for its comparison with the corresponding synthetic or estimated one.

The water particle excursion or Lagrangian paths, induced by the time evolution of the velocity field

during the first 6 h after the arrival of the tsunami, ranged from 1 to 6 km by the harbor entrance in the upper threshold scenario, while excursion paths are in general less than 0.5 km in the lower threshold scenario. In particular, in the upper threshold scenario, Lagrangian paths are indicating a large eddy like circulation outside the harbor entrance (2 km in diameter, Fig. 3). Furthermore, typical of a simple model basin with narrow strait, two pair of transient vortices are revealed in both case-scenarios (Fig. 4) by employing the mathematical concept of residual velocity (the time-average of velocity field; e.g., Imasato 1983) despite of the complex geometry of the harbor.

Outside the harbor, in Todos Santos Bay in which the Port of Ensenada is located, the resulting currents in the upper threshold scenario (Fig. 5), are found to be 2–3 knots along the eastern side of the bay

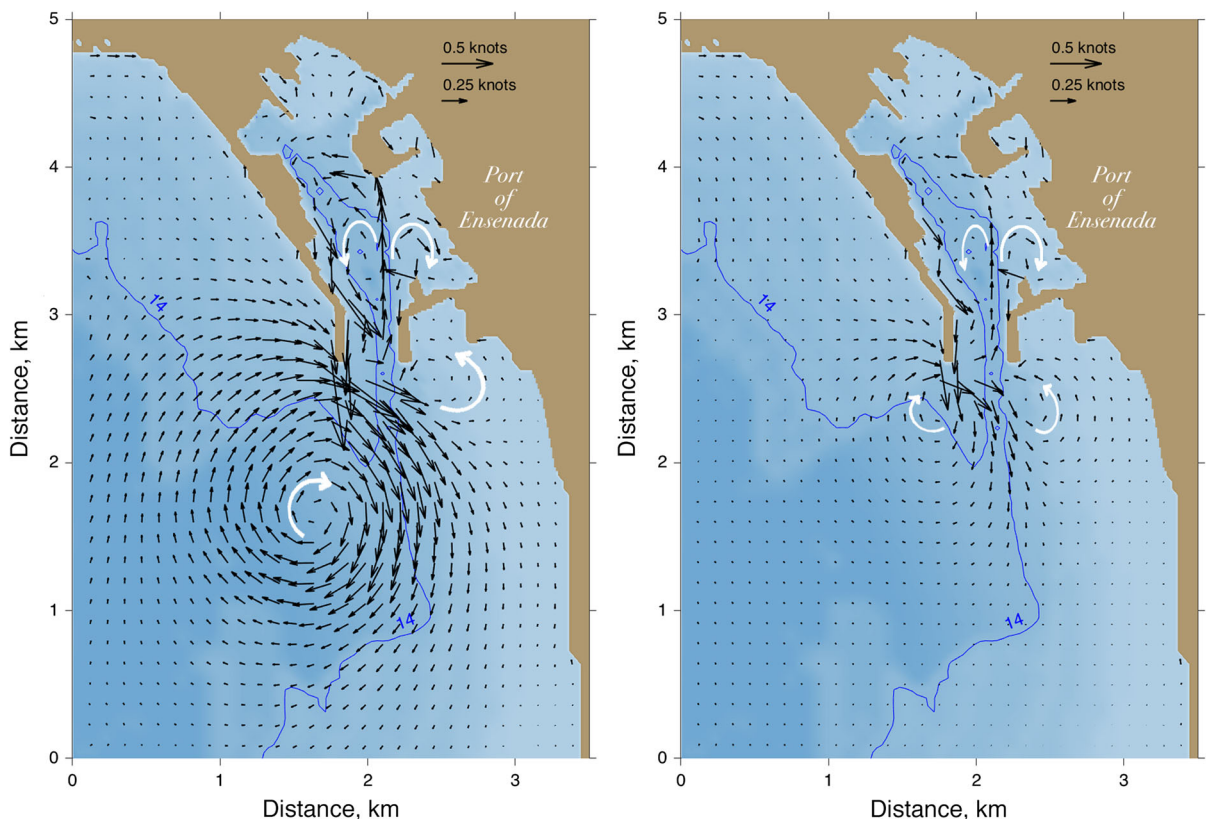


Figure 4

Residual velocity field inside and outside the harbor (left panel, upper threshold scenario; right panel, lower threshold scenario). White arrows highlight the two pair of transient vortices revealed by the residual velocity field. Residual velocity fields were computed by the time-average of the first 6 h of the velocity field after the tsunami arrival

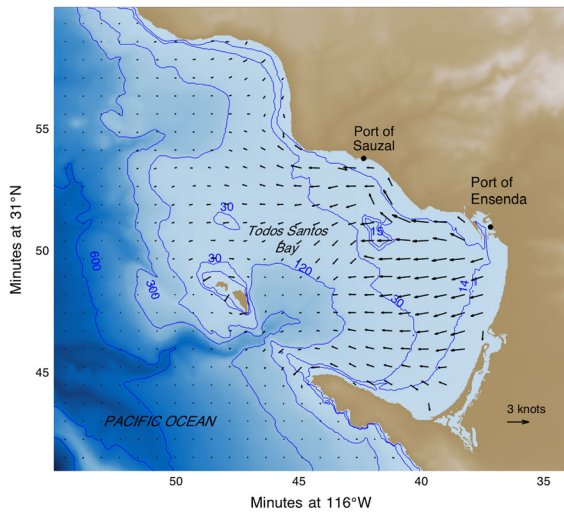


Figure 5

Upper threshold scenario: maximum tsunami-induced currents in Todos Santos Bay, whether it corresponds to flow or ebb. Blue lines indicate isobaths, depths in meters. Note that ebb currents exceed flood currents, as illustrated in Fig. 3

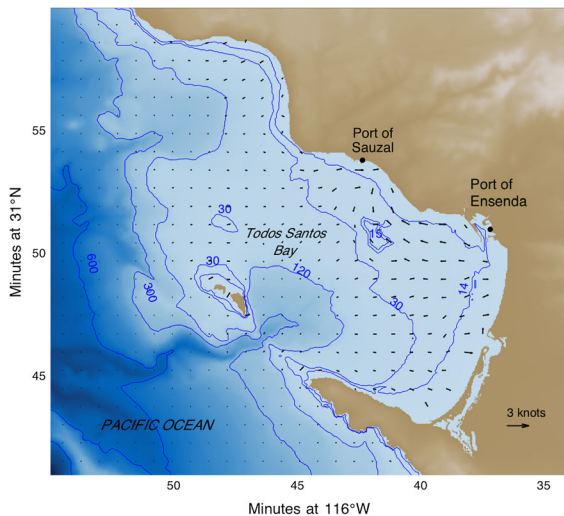


Figure 6

Lower threshold scenario: maximum tsunami-induced currents in Todos Santos Bay, whether it corresponds to flow or ebb. Blue lines indicate isobaths, depths in meters

between the 14 and 30 m isobaths, and are less than 2 knots in depths greater than 30 m. In contrast, the resulting currents in the lower threshold scenario (Fig. 6), are less than 2 knots between the 14 and 30 m isobaths, and practically negligible at depths greater than 30 m. In both case scenarios, currents are practically negligible at depths greater than 120 m (15 km offshore from the harbor).

#### 4. Coastal Seiches and Currents in the Port of Ensenada

It is well known that tsunamis originated in different regions around the Pacific have the same sea level spectral shape in a specific bay or harbor due to the natural local resonant eigen-modes or coastal seiches (e.g., Rabinovich 1997; Zaytsev et al. 2017), i.e., in the Port of Ensenada, the sea level variance during the Tohoku 2011 tsunami was found largely amplified in the whole spectrum while keeping the spectral shape of the background sea level spectrum at the periods  $T \sim [51, 29, 21, 6, \text{ and } 3 \text{ min}]$  (cf. Fig. 7, in Zaytsev et al. 2017). In particular, the harbor sea level frequency response in the Port of Ensenada, as computed by the spectral ratio (admittance and coherence; Fig. 7a–c) between the synthetic tsunami records, at the tide gauge location, and at 2 km outside the harbor (both records resulting from the Tohoku 2011 tsunami model, Eqs. 3, 4) reveals two resonant periods with an amplification factor of 3.5 centered at the period of 21 min, and an amplification factor of 2.5 at the period of 6.7 min.

The period  $T_0 = 21 \text{ min}$  may correspond to the fundamental zeroth Helmholtz longitudinal mode, which is also called the pumping mode because it is related to periodic mass transport—pumping—through the harbor entrance (e.g., Rabinovich 2009); while the period at  $T_1 = 6.7 \text{ min} \cong T_0/3$  may correspond to the period of the first Helmholtz longitudinal mode according to the formula  $T_n = 4L/(2n + 1)/\sqrt{gh}$  for modes  $n = 0, 1, \dots$  in a rectangular open-mouth basin.

In order to illustrate the profiles of sea level and currents along the harbor axis, corresponding to both resonant periods, harmonic water-level variations with a moderate wave height ( $H = 0.2 \text{ m}$ ) were introduced as forced boundary condition in an artificial channel towards the harbor entrance in the hydrodynamic numerical model of Goto et al. (1997), applicable to the Port of Ensenada (Eqs. 3, 4; Fig. 8) in a matrix of  $201 \times 454$  nodes with a grid resolution of 10 m. The resulting profiles of sea level and currents along the harbor axis corresponding to both resonant periods are illustrated in Fig. 9.

The high coherence level for periods longer than 19 min (Fig. 7c), indicate that these periods

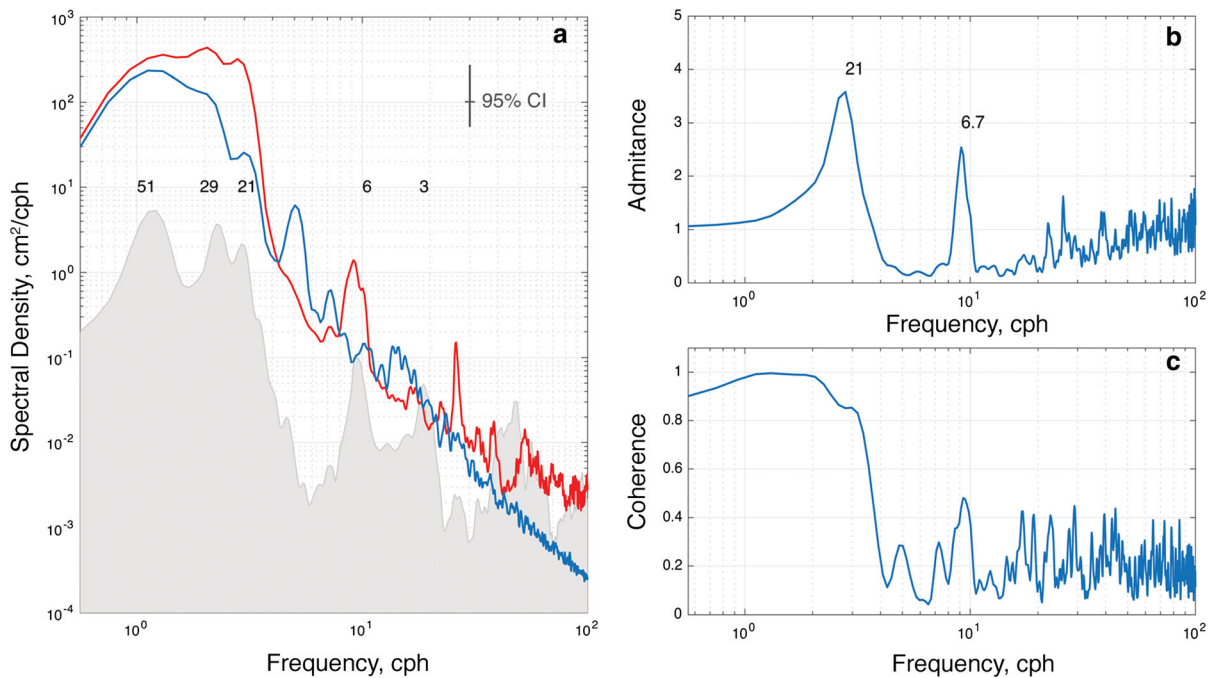


Figure 7

Sea level Spectral Density: **a** Background Spectrum (shaded area) obtained from the recorded sea level in the Port of Ensenada at the tide gauge location in an ordinary day, in comparison with the Spectra obtained from the model results of the Tohoku 2011 tsunami inside (red) and outside (blue) the port; **b**, **c** Admittance and coherence between the inside and outside tsunami records

correspond to coastal seiches originated outside the harbor where the resonant period  $T_0 = 21$  min corresponds to both, a harbor seiche, as well as to a coastal seiche outside the harbor. The low coherence level at the resonant period  $T_1 = 6.7$  min indicates that this period corresponds to a harbor seiche, that besides of being excited by sea level fluctuations outside the harbor, is also excited by the multiple wave reflections within the complex harbor geometry.

It is noticeable the lack of variance in the sea level spectrum at 6 cph ( $T = 10$  min) in both, the background spectrum, and in the Tohoku 2011 tsunami spectrum at the tide gauge location in the Port of Ensenada (Fig. 7a; cf. Fig. 7, in Zaytsev et al. 2017). This is because the nodal line of the harbor resonant mode ( $T_0 = 21$  min), which is located outside the harbor (Fig. 9a), migrates towards the tide gauge

location (location 12 along the harbor axis in Fig. 8) as the period of the forcing waves decreases. Shorter wave periods move forward the nodal line up to the location 15 (Fig. 9c), where the nodal line corresponding to the period  $T_1 = 6.7$  min is located.

An approximate insight of the spectral and spatial structure of seiches outside the harbor is given here by the empirical orthogonal functions (EOF; e.g., Tolkova and Power 2011; Aránguiz 2015) of the sea level time history resulting from the numerical modeling of the Tohoku 2011 tsunami. The first EOF, the one with the largest variance (35%), has a composed spectrum (Fig. 10a) with a dominant peak at the period 60 min, and a secondary peak centered at 20 min. By speculation, its spatial structure (Fig. 10b) resembles a fundamental zeroth Helmholtz longitudinal mode in Todos Santos Bay. The second EOF (variance 33%) has a composed spectrum



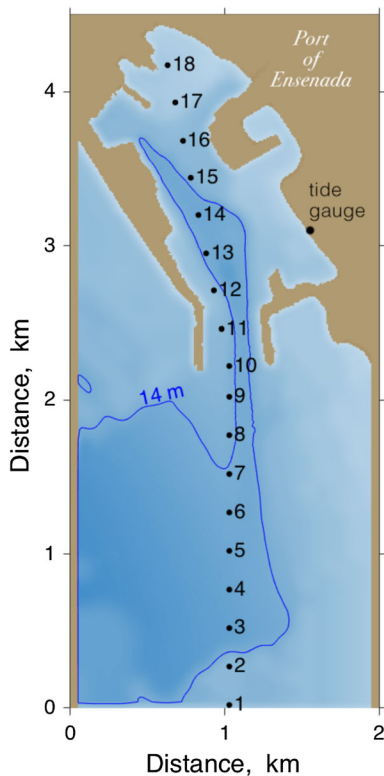


Figure 8

Artificial channel towards the Port of Ensenada with an open boundary at the channel mouth. Dots are indicating 18 locations along the channel and harbor axis. The 14 meters isobath is indicated in blue

(Fig. 10c) with two dominant peaks at 30 and 60 min, and a secondary peak centered at 20 min; its spatial structure (Fig. 10d) resembles a “continental shelf trapped tsunami mode”. The variance (10%) of the third EOF is distributed in a narrow spectral band between 20 and 30 min (Fig. 11a), while its spatial structure (Fig. 11b) resembles a series of coastal trapped waves, which might be a result of transient “coastal trapped edge waves tsunami modes” (e.g., González et al. 1995), captured by the orthogonal decomposition method. The variance (6%) of the fourth EOF is distributed in a wide spectral band between 10 and 60 min, which makes difficult its physical interpretation. It is noticeable that a spectral peak appears in all of the EOFs near the fundamental harbor resonant period ( $T_0 = 21$  min).

## 5. Discussion and Conclusions

As a result of coastal and harbor seiches, a large number of significant waves ( $H > 1$  m) are observed in the tsunami records of the Chile 1960, Alaska 1964, and Tohoku 2011 tsunamis for more than 24 h after the tsunami arrivals (Fig. 2), consequently, large flood and ebb currents (4–6 knots, as the ones illustrated in Fig. 3) can be expected to occur by the harbor entrance during the same period of time that would make navigation difficult inside and around the harbor for several hours after the arrival of a tsunami. Moreover, tsunami heights greater than 1.5 m above the still water-level would represent a considerable hazard if the tsunami were to arrive during the spring tides, as the piers in the harbor are 1.5 meters above the Mean Higher High Water (MHHW) and 1.23 m above the Mean Spring Tide Level (MSTL, defined here as the average of the maximum heights observed during consecutive spring tide cycles).

Low amplitude tsunamis ( $H_s = 0.69$ – $0.79$  m), as the ones illustrated in Fig. 2; Table 1, may not represent inundation hazard, however, those may produce important currents of 2–3 knots at the harbor entrance as a result of the interaction of coastal and harbor seiches that may excite the natural harbor seiches at the resonant periods  $T_0 = 21$  min, and  $T_1 = 6.7$  min (e.g., Figs. 7, 8). Note that the lowest amplitude recorded tsunami (Chile 2015) has a significant wave height and period ( $H_s = 0.22$  m;  $T_s = 24$  min) similar to those of the forced boundary condition ( $H = 0.2$  m;  $T = 21$  min) at the mouth of the artificial channel in Fig. 9, that in turn produced currents of  $\sim 1.5$  knots at the harbor entrance and wave heights of  $\sim 1$  m at the harbor head (Figs. 8a, b).

Figures 3, 4, 5 and 6 of maximum expected tsunami-induced currents mapped inside and outside the Port of Ensenada, were carefully confectioned for practical use to anticipate harbor operations, as well as to identify safety maritime evacuation zones. However, whether estimated tsunami-induced currents may be considered a hazard to navigation or harbor operations will depend on the judgement of navigators and port authorities.

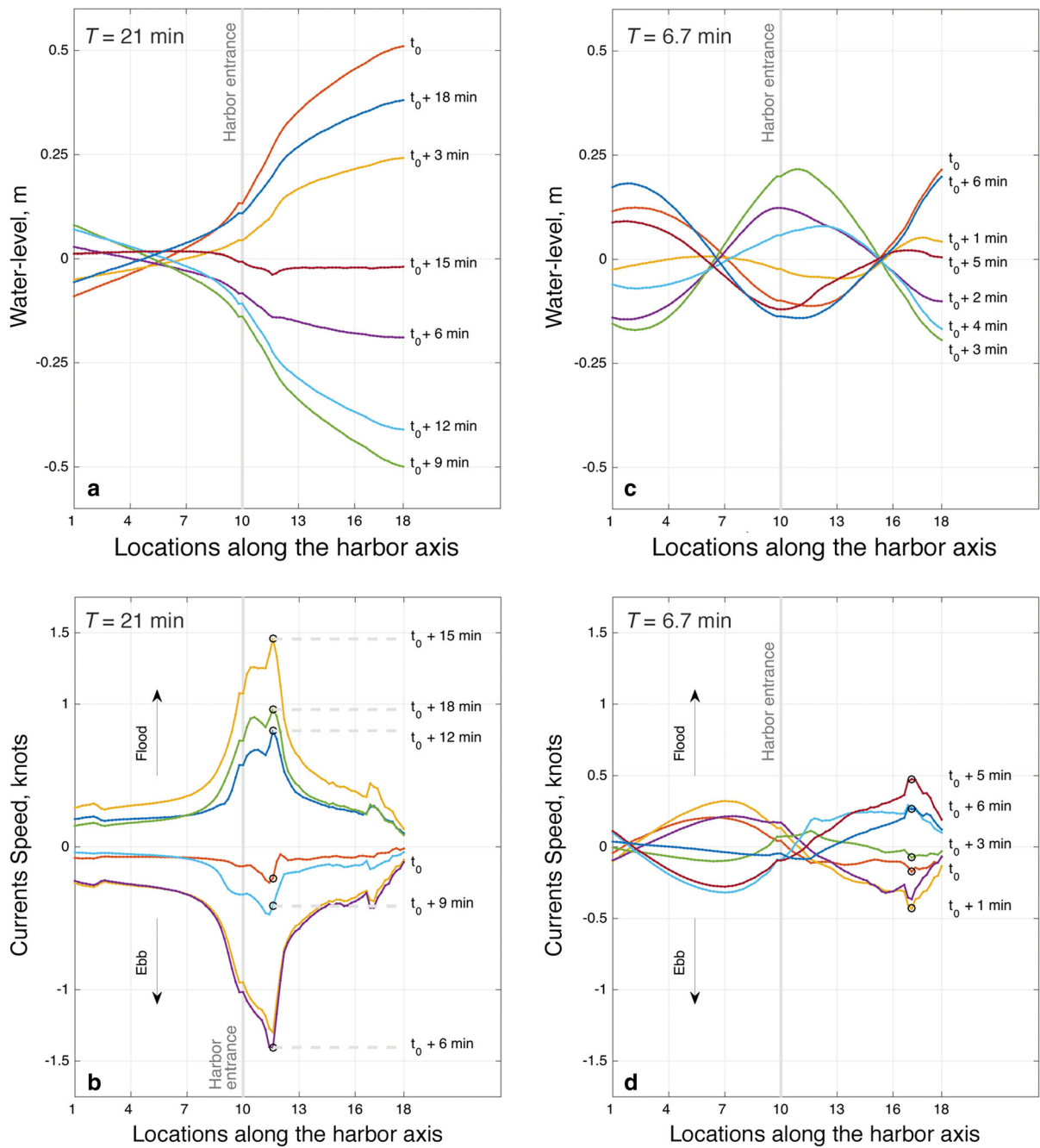


Figure 9

Profiles of water-level and currents along the harbor axis within one wave period: **a, b** for the resonant period  $T = 21$  min; **c, d** for the resonant period  $T = 6.7$  min. Colors to easily follow single profiles

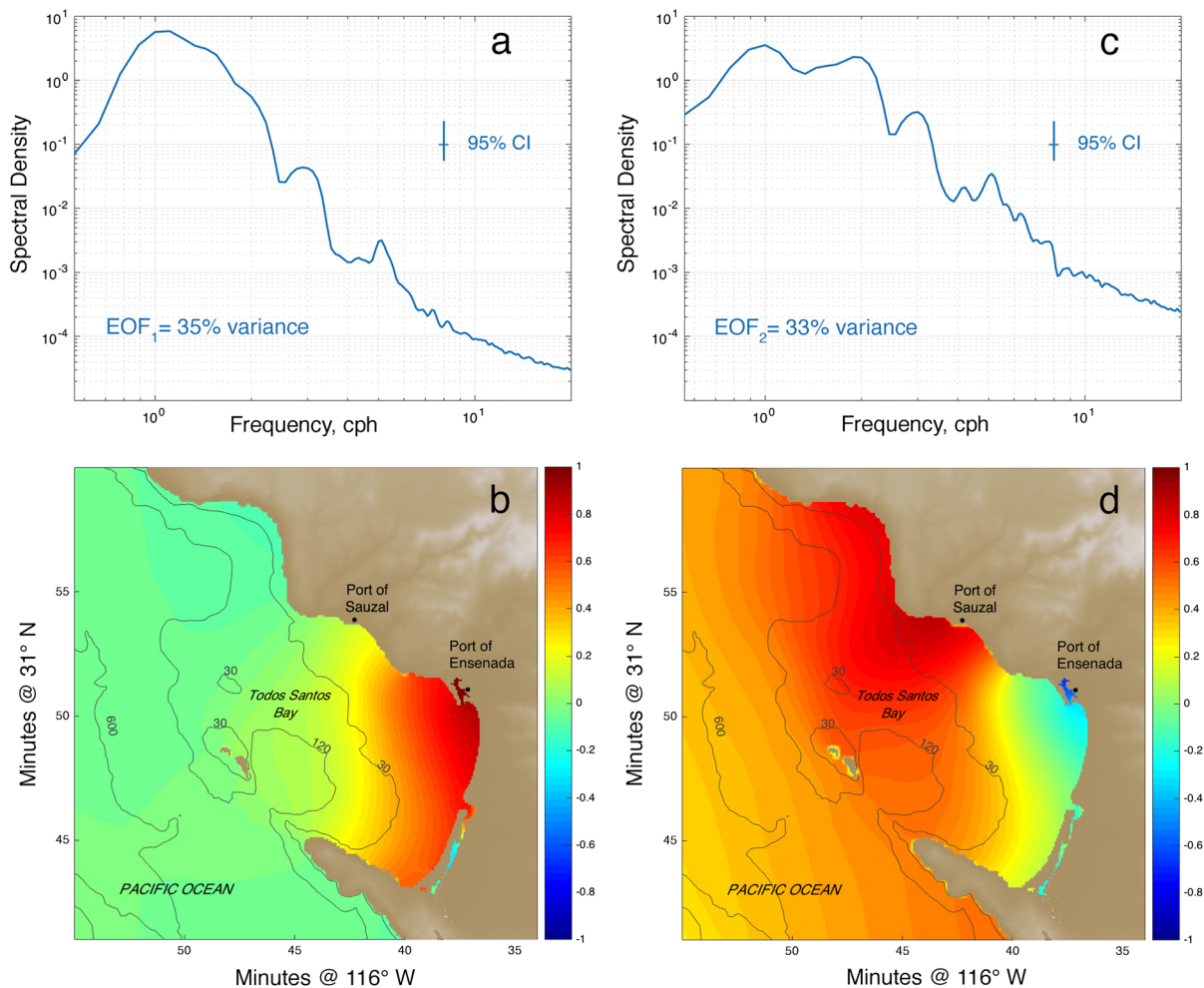


Figure 10

Spectral and spatial distribution of the first (a, b) and second (c, d) EOFs. Spectral density weighted by the corresponding percentage of variance. Color scale indicate the corresponding normalized amplitude of the EOFs spatial distribution. Contour lines indicate isobaths with depths annotated in meters

It is of a practical use to close a harbor to navigation after a tsunami warning is issued. However, reopen it to navigation would depend on the magnitude of the tsunami-induced currents and sea-level variations inside and around the harbor for the safety of navigation. Therefore, it would be desirable for a modern port to deploy an adequate array of pressure-gauges and current-meters operating in real time for marine traffic control to be able to close or reopen

port operations to prevent damage and economic losses (e.g., <https://tidesandcurrents.noaa.gov/ports>).

In addition, tide-induced currents were computed by introducing the tide level of one tidal day during the spring tides (1.6 m peak to trough) at the harbor entrance in the numerical model (Eqs. 3, 4; Fig. 8). The resulting currents (0.2 knots) are representative of the natural background currents in the harbor, and served as a reference frame for the magnitude of the tsunami-induced currents estimated above.

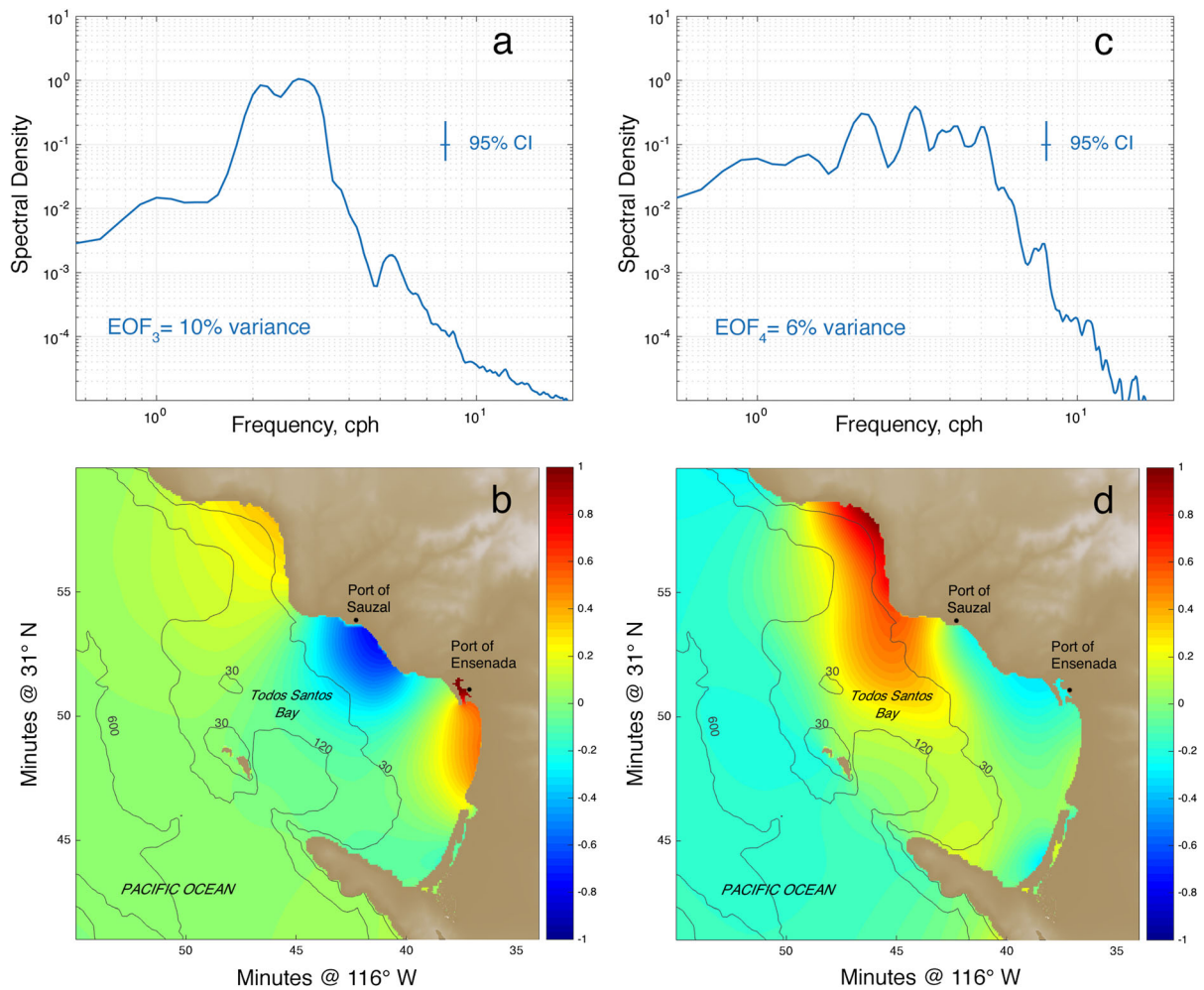


Figure 11

Spectral and spatial distribution of the third (a, b) and fourth (c, d) EOFs. Spectral density weighted by the corresponding percentage of variance. Color scale indicate the corresponding normalized amplitude of the EOFs spatial distribution. Contour lines indicate isobaths with depths annotated in meters

### Acknowledgements

To CONACyT (México) through the Ph.D. program scholarship CVU221676 that made this study possible. Tsunami records courtesy of the Joint Sea Level Network Operations of Mexico, operated by CICESE, IMT, SEMAR, and UNAM. ETOPO2v2 bathymetric data courtesy of the National Geophysical Data Center (2006). High-resolution bathymetric data around the Port of Ensenada courtesy of the Division of Coasts and Harbors of the Mexican Institute of Transportation (IMT). Thanks to both

anonymous reviewers and the Editor for their sound and constructive comments that enhanced the contents of the manuscript, and to Professor Modesto Ortiz for the fruitful discussions throughout this study.

### Funding

This study was funded by Consejo Nacional de Ciencia y Tecnología (Grant No. 221676).

**Publisher's Note** Springer Nature remains neutral with regard to jurisdictional claims in published maps and institutional affiliations.

#### REFERENCES

- Aránguiz, R., (2015). *Tsunami Resonance in the Bay of Concepción (Chile) and the effect of Future Event*. Handbook of Coastal Disaster Mitigation for Engineers and Planners. <http://dx.doi.org/10.1016/B978-0-12-801060-0.00006-X>.
- Arcos, M. E. M., & LeVeque, R. J. (2015). Validating velocities in the GeoClaw tsunami model using observations near Hawaii from the 2011 Tohoku tsunami. *Pure and Applied Geophysics*, 172(3–4), 849–867. <https://doi.org/10.1007/s00024-014-0980-y>.
- Dronkers, J. J. (1964). *Tidal computations in rivers and coastal waters*. Amsterdam: North-Holland Publishing Company.
- González, F. I., Satake, K., Boss, E. F., & Mofjeld, H. O. (1995). Edge wave and non-trapped modes of the 25 April 1992 Cape Mendocino tsunami. *Pure and Applied Geophysics*, 144(3–4), 409–426. <https://doi.org/10.1007/BF00874375>.
- Goto, C., Ogawa, Y., Shuto, N., and Imamura, F. (1997). IUGG/IOC Time Project, in IOC Manuals and Guides No. 35, UNESCO, Paris.
- Imasato, N. (1983). What is tide-induced residual current? *Journal of Physical Oceanography*, 13(7), 1307–1317. [https://doi.org/10.1175/1520-0485\(1983\)013%3c1307:WITIRC%3e2.0.CO;2](https://doi.org/10.1175/1520-0485(1983)013%3c1307:WITIRC%3e2.0.CO;2).
- ITSU Master Plan, (1999). *Tsunami Warning System in the Pacific Master Plan*. Intergovernmental Oceanographic Commission (IOC) of UNESCO.
- Mansinha, L., & Smylie, D. E. (1971). The displacement fields of inclined faults. *Bulletin of the Seismological Society of America*, 61(5), 1433–1440.
- National Geophysical Data Center. (2006). 2-minute Gridded Global Relief Data (ETOPO2) v2. *National Geophysical Data Center, NOAA*. <https://doi.org/10.7289/v5j1012q>.
- Ortiz-Huerta, L. G., Ortiz, M., & García-Gastélum, A. (2018). Far-field tsunami hazard assessment along the Pacific coast of Mexico by historical records and numerical simulation. *Pure and Applied Geophysics*, 175(4), 1305–1323. <https://doi.org/10.1007/s00024-018-1816-y>.
- Pedlosky, J. (1979). *Geophysical fluid dynamics*. New York: Springer. <https://doi.org/10.1007/978-1-4684-0071-7>.
- Rabinovich, A. B. (1997). Spectral analysis of tsunami waves: Separation of source and topography effects. *Journal of Geophysical Research: Oceans*, 102(C6), 12663–12676.
- Rabinovich, A. B. (2009) “Seiches and harbor oscillations,” Handbook of Coastal and Ocean Engineering, ed. Kim, Y. C. (World Scientific, Singapore), pp. 193–236. [https://doi.org/10.1142/9789812819307\\_0009](https://doi.org/10.1142/9789812819307_0009).
- Titov, V.V., González, F.I., Mofjeld, H.O., & Venturato, A.J. (2003). NOAA time seattle tsunami mapping project: procedures, data sources, and products. US Department of Commerce, National Oceanic and Atmospheric Administration, Oceanic and Atmospheric Research Laboratories, Pacific Marine Environmental Laboratory.
- Tolkova, E., & Power, W. (2011). Obtaining natural oscillatory modes of bays and harbors via Empirical Orthogonal Function analysis of tsunami wave fields. *Ocean Dynamics*, 61(6), 731–751. <https://doi.org/10.1007/s10236-011-0388-5>.
- Zaytsev, O., Rabinovich, A. B., & Thomson, R. E. (2017). The 2011 Tohoku tsunami on the coast of Mexico: A case study. *Pure and Applied Geophysics*, 174(8), 2961–2986. <https://doi.org/10.1007/s00024-017-1593-z>.

(Received April 12, 2019, revised August 13, 2019, accepted August 14, 2019, Published online September 9, 2019)